Marc Röger
German Aerospace Center (DLR),
Solar Research,
Plataforma Solar de Almería,
Tabernas 04200, Spain
e-mail: marc.roeger@dlr.de

Patrik Herrmann
Technical University of Darmstadt,
Reactive Flows and Diagnostics,
Darmstadt 64287, Germany

Steffen Ulmer
German Aerospace Center (DLR),
Solar Research,
Plataforma Solar de Almería,
Tabernas 04200, Spain

Miriam Ebert
German Aerospace Center (DLR),
Solar Research,
Plataforma Solar de Almería,
Tabernas 04200, Spain

Christoph Prahl
German Aerospace Center (DLR),
Solar Research,
Plataforma Solar de Almería,
Tabernas 04200, Spain

Felix Göhring
German Aerospace Center (DLR),
Solar Research,
Cologne 51147, Germany

Techniques to Measure Solar Flux Density Distribution on Large-Scale Receivers

Flux density measurement applied to central receiver systems delivers the spatial distribution of the concentrated solar radiation on the receiver aperture, measures receiver input power, and monitors and might control heliostat aimpoints. Commercial solar tower plants have much larger aperture surfaces than the receiver prototypes tested in earlier research and development (R&D) projects. Existing methods to measure the solar flux density in the receiver aperture face new challenges regarding the receiver size. Also, the requirements regarding costs, accuracy, spatial resolution, and measuring speed are different. This paper summarizes existent concepts, presents recent research results for techniques that can be applied to large-scale receivers and assesses them against a catalog of requirements. Direct and indirect moving bar techniques offer high measurement accuracy, but also have the disadvantage of large moving parts on a solar tower. In the case of external receivers, measuring directly on receiver surfaces avoids moving parts and allows continuous measurement but may be not as precise. This promising technique requires proper scientific evaluation due to specific reflectance properties of current receiver materials. Measurement-supported simulation techniques can also be applied to cavity receivers without installing moving parts. They have reasonable uncertainties under ideal conditions and require comparatively low effort. [DOI: 10.1115/1.4027261]

Keywords: flux density measurement, receiver input power, central receiver system, solar tower

1 Introduction

Flux density measurement techniques on large-scale receivers of central receiver systems deliver the receiver input power that is necessary to get performance figures of receiver and heliostat field. Moreover, continuous measurement of the flux density distribution facilitates efficient receiver operation and heliostat aimpoint control. Different receiver types and requirements regarding the measurement purpose result in several possible solutions for flux measurement on large-scale receivers.

The measurement techniques regarded in this paper can be classified in indirect, direct, and measurement-supported simulation methods. While indirect methods use digital cameras to measure the solar radiation reflected off a surface, the direct methods use flux sensors that directly deliver a measurement signal proportional to the irradiative flux. Simulation methods may also be used to get highly resolved solar flux maps. Either direct or indirect simplified measurement methods can serve as validation of the simulations. As only serving to validate the simulations and not being result, the measurements can be reduced in resolution and complexity in this case.

There are two basic receiver types: external receivers, whose absorber surface more or less equals the aperture surface, and cavity receivers, whose aperture is not identical to the absorber surfaces. In the first case, the external receiver surface may be used as a measurement target with the camera being located in a secure distance to the receiver. In the second case (cavity receivers), images of all the surfaces inside the receiver cavity must be available that would imply the installation of several cameras near or inside the receiver and the effect of reflection of solar radiation inside the cavity must be considered. For that reason, cavity receivers may require a different measurement approach.

2 State-of-the-Art: Flux Density Measurement on Prototype-Scale Receivers

2.1 Methods. Several indirect methods (camera-target) and direct methods (sensors) to measure the flux distribution have been proposed:

(i) white diffuse moving bar target and digital camera
(ii) digital camera only without target applied to external receivers
(iii) stationary stripe-shaped target, digital camera, and moving focus
(iv) sensors mounted on moving bar
(v) distributed and stationary sensors

Additionally, ray tracing simulations have been used to provide flux density distributions during layout and operation of plants. During the last decades, prototype-scale receivers and heliostat fields have been characterized by techniques (i), (iv), and (v),

Contributed by the Solar Energy Division of ASME for publication in the Journal of Solar Energy Engineering. Manuscript received March 1, 2012; final manuscript received March 7, 2014; published online May 2, 2014. Editor: Gilles Flamant.

whereas techniques (ii) and (iii) are still in the development phase and have been applied only to few receivers.

(i) The widespread camera target methods (indirect method) uses either charged coupled device (CCD) or complementary metal–oxide–semiconductor cameras that record the flux brightness distribution on a white diffusely reflecting target placed in front of the receiver surface. Due to their high dynamic range and signal quality, often CCD cameras are used. The intensity of reflected solar light is calibrated using a solar flux gauge. Advantages of this method are its very high spatial resolution, short measurement time, high reliability, and the possibility to calibrate with one solar flux gauge. This measurement principle was used since the end of the 1970s worldwide in different R&D central receiver projects, e.g., Beam Characterization System (BCS) of Sandia (USA) [1], Flux Analyzing System of EIR (Switzerland) [2], heliostat and receiver measurement system (HERMES I + II, ProHERMES) of the German Aerospace Center (DLR) Plataforma Solar de Almeria (PSA) [3–5], and [1]CSIRO (Australia) [6], in solar furnaces, e.g., [2]FATMES and [3]SCATMES of DLR Cologne [7,8], OBELIX of [4]CNRS France [9], and in Dish/Stirling systems [10,11].
In case there is no large Lambertian target, often a moving bar is used to scan the whole focal area while a camera takes several photos (e.g., the ProHERMES system at the Plataforma Solar de Almería (PSA) [5]). After image acquisition and deskewing, the target region is cropped in each image and combined to a surface covering the whole region of interest. The resulting image is corrected for camera nonlinearities, dark current, and shading and is finally calibrated by a radiometer. Due to ageing and soiling of the white reflective target and radiometer, a periodic recalibration should be foreseen. The ProHERMES moving bar has been working without mechanical problems.
Having corrected systematic uncertainties, Ulmer et al. [12,13] report a low total measurement uncertainty of solar flux density, being in the range from −4.7% to +4.1% for the ProHERMES system. Strachan and Houser [14] reports for the BCS a total error of about 6%, being the calibration uncertainty of the flux gauge the principal source of uncertainty (5%). Also Ulmer [12] identifies the flux gauge calibration as the highest contribution and assumes about ±3%. Further relevant uncertainties to measurement of flux density distribution on the receiver aperture plane are the distance between the measurement plane and aperture plane in interest (±1% after simulation based correction), spectral effects (±1% using both neutral density and heat control filters and after corrections), and uncertainties in positioning (±2%) and sizing (±1%) during image processing [12]. A periodic calibration is regarded as indispensable to account for the degradation of the radiometer paint and the white Lambertian surface of the moving bar.

(ii) In the case of external receivers, the receiver surface itself can be used as measurement target. This indirect method overcomes an additional moving bar installation and calibrates the intensities reflected off the images of the receiver surface. Some tests performed at the PSA in the years 2007 and 2008 during operation of a 3-MWth open volumetric receiver are reported in Sec. 3.
The PHLUX method by Ho and Khalsa [15] uses a recorded image of the sun, a direct normal irradiance (DNI) reading, and the reflectivity of the target or receiver to calibrate the brightness distribution of target or receiver surfaces. A heliostat beam flux map on a Lambertian surface was measured with an error in the peak flux of 2% relative to a flux-gauge measurement when the filter attenuation factors and effective receiver reflectivity were characterized. However, applied to external receiver surfaces, filter attenuation values different from the manufacturer's specifications, spectral dependencies, and uncertainty in receiver reflectivity may increase measurement uncertainty significantly (up to 20–40%) [15].
Techniques using the receiver surface as measurement target could also be transferred to cavity receivers, provided that the camera sees the whole receiver cavity surfaces. However, several cameras, partly in hot receiver regions, might be necessary and the effect of reflection of solar radiation inside the cavity must be considered.

(iii) Another indirect method first mentioned in Ref. [16] is to use a stationary stripe-shaped target and sweeping the focus over the fixed target. No mechanical parts have to be installed near the focus. The stripe-shaped images are then merged to gain a composite flux image. Pacheco et al. [16] report a test with 30 heliostats moved over a horizontally oriented stripe target. The actual target was large enough to fit the whole beam spot, but only a stripe was considered. The aimpoint was moved in 0.4 m steps to measure the 2.0 m beam spot. The time required to achieve the new aimpoint was about 15 s. Analyses of the composite image indicate that the total power, peak power, and beam size were within 2% of the reference which was the mean of all images which made up the composite.

(iv) A moving bar can also be equipped with sensors that scan the aperture surface during the movement. Gardon flux gauges are thermal sensors with high response times. The scan would take several minutes, resulting in the necessity of active water cooling of moving bar and sensors. For this reason, Ballestrín and Monterreal [17] used in their MDF system (Medida Directa de Flujo) thin film heat flux sensors having fast time constants in the range of microseconds and allowing a rapid scan without water cooling. They can operate up to 850 °C and measure heat flux and temperature by creating a small temperature difference across the thermal resistance element of a thermopile. For the application in solar heat flux measurement, they were painted with a black painting (Zynolte™) with an absorptance of approximately 94%. Being a direct measurement method, uncertainties caused by camera and target properties are avoided. The accuracy of the heat flux microsensors is reported to be ±3%. Due to their small size, numerous of these sensors can be mounted along the moving bar. Additionally, available high frequency data acquisition systems allow a high density of measurement points along the moving bar scan path without reducing the bar speed and excessive heating of the sensors. This results in a rather good spatial resolution for direct measurement systems and allows relatively low interpolation errors. With eight heat flux sensors having distances between 50 mm and 150 mm along the moving bar and a mean spacing of measurement points along the moving bar scan path of 11 mm, Ref. [17] reports an accuracy of about 6% in their tests.
Based on the work of Ballestrín et al. [17], eSolar designed, built and tested a pneumatically actuated, 6.1 m long rotary moving bar equipped with several thin film heat flux sensors in their plant [18], capable of measuring flux densities up to 5 MW/m^2. Additionally, they integrated the possibility of measuring heat flux by an indirect method using a remote camera and the moving bar being covered by a white refractory. They report a good performance of the system during the in-field testing.
Elsayed et al. [19] used a two-dimensional traverse mechanism to move an uncooled alphatometer (Devices and Services) to study the flux distribution of a small heliostat.

[1]Commonwealth Scientific and Industrial Research Organisation (CSIRO)
[2]Flux And Temperature MEasurement System (FATMES)
[3]Scanning Camera and Target Measurment System (SCATMES)
[4]French National Centre for Scientific Research (CNRS)

(v) Moving parts are avoided if several water-cooled flux gauges are distributed in the aperture plane or on the receiver surface. Heat flux maps can be created by interpolation between the measurement points. Numerous sensors are required to get accurate results. Nonequal sensor distribution over the measurement surface allows the reduction of sensor number while maintaining a reasonable measurement uncertainty. Stationary sensors were used, for example, at the PS-10 plant in Seville [20]. As being a direct method, measurement accuracy at sensor locations is high; however, spatial resolution may only be moderate while not using excessive numbers of sensors. Maintaining the reliable operation of high numbers of sensors in high-flux high-temperature receiver zones over the lifetime of a receiver is a challenging task. Experience has shown that the lifetime of flux gauges in the receiver environment is about 6 months [16].
Another possibility that can be classified as a stationary sensor method is described in Lewandowski et al. [21]. They used a nickel wire mesh that is placed in the solar focus. The wire mesh heats and the wires change their electric resistance. Assuming a Gaussian flux distribution and using the laws of radiation exchange, the flux distribution can be calculated. Continuous online measurement without disturbing receiver operation is possible. The drawback is the relatively high measurement uncertainty due to wind effects, thermal emission and reflection from the receiver, and nonconstant wire material properties. Additionally, the measurement is restricted to already known flux distributions (e.g., Gaussian) and the wire lifetime is limited.

Finally, state-of-the-art ray tracing codes allow a very accurate prediction of the solar flux on any surface. Accuracy of results depends mainly on the quality of input parameters. Ray tracing results should be validated by measurements that may be reduced in complexity and accuracy (see Sec. 3.6)

2.2 Calibration of Sensors and Digital Flux Images. Sensors like the most commonly used Gardon-type radiometers (Vatell™) must be calibrated to measure directly the solar flux or to be used for calibration of brightness maps provided by digital cameras. This is because the manufacturer's calibration method differs in the spectral composition and angles of incidence from the solar use [13]. Kaluza and Neumann [22] report the experiences of an international comparison campaign between different solar flux gauges in a solar furnace using Kendall or calorimetric radiometers as reference.

Ballestrín et al. [23] suggest a calibration method that uses the Gardon sensor as calorimeter by measuring inlet and outlet cooling water temperatures. As an electrically heated furnace is used, the calibration constants are corrected to be used with solar radiation. The achieved measurement uncertainties are estimated in the range of 2% [23].

Ho and Khalsa [15] present a new method (PHLUX) that does not require flux gauges or calorimeters to calibrate digital brightness images. Instead, it uses a recorded image of the sun, a DNI reading, and the reflectivity of the target or receiver. The image of the sun can also be used to provide a spatial reference to quantify the physical size of the flux map. Due to saturation, different neutral density filters for the receiver flux map and the image of the sun might be used.

3 Flux Density Measurement Techniques for Large-Scale Receivers

This section presents some recent work of the German Aerospace Center (DLR) focused on the up-scaling of existent concepts and on techniques in the development phase.

3.1 Flux Density Measurement by Using a White Diffuse Moving Bar Target and Digital Camera. Rotating moving bars are a good choice for small-scale prototype receivers, because only one drive is necessary at the rotating axis, which results only in one small opening in the front protection of the tower. However, the up-scaling of rotational moving bars is critical because of the high angular momentums and the influence of wind. A counterweight is possible, but increases total weight and inertia of the system.

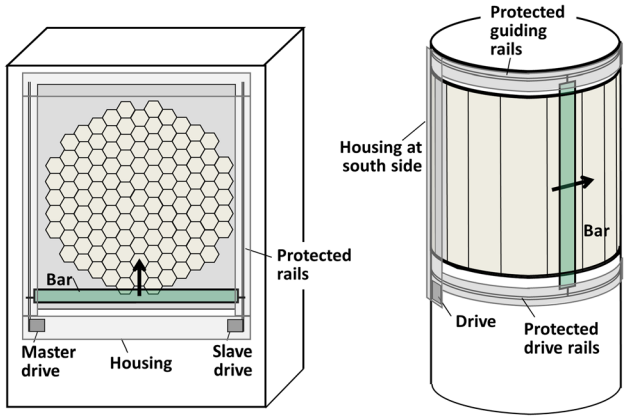

Fig. 1 Possible mechanisms of linear moving bars (left: horizontal bar and right: vertical bar)

Up-scaling should be possible by switching over to a concept with linear movement of the bar (Fig. 1). Issues of thermal expansion and thermal load by convection of hot air and radiation have to be considered in the design process. External surround receivers may be equipped preferably by vertical linear moving bars, which are moved along the circumferential receiver line. The drive should be located at the bottom of the receiver with sufficient distance to avoid the exposure to hot convection air flows and should be protected against concentrated solar radiation. The upper part may only be guided in a rail or rod to avoid temperature sensitive drives and motors in this region. Depending on the angle of acceptance of the receiver, several cameras are needed on ground. Alternatively, a single moving camera mounted on the lower end of the moving bar can be used.

In the case of cavity receivers, usually there is enough space on both sides of the receiver to mount guiding rails. A feasible option is a horizontal linear moving bar with two motors operated in master/slave. The two drives and rails are outside of high-solar-flux regions or hot air convection zones and can be protected adequately against the lower solar fluxes. Master/slave operation helps to avoid tilting of the moving bar. For all systems, measurement accuracy should be comparable to the ProHERMES system (-4.7% to $+4.1\%$).

3.2 Flux Density Measurement on External Receiver Surfaces Using a Digital Camera. External receiver surfaces may be used as measurement targets if they reflect more or less diffusely (not specularly) and there is no pronounced height profile of the receiver surface. The tests reported in this paper have been performed at the PSA during operation of a 3-MWth open volumetric receiver.

Special attention has to be drawn to the difference in the scales of reflected solar radiation and emitted thermal radiation compared to flux density measurement on a white moving bar target (Sec. 3.1). A moving bar target is highly reflective and its temperature is usually low. In contrast, a high-temperature receiver surface has a low reflectivity and is highly emitting that may bias the signal of solar radiation on the CCD camera chip. A spectral filter that cuts off radiation with wavelengths above 0.6 μm is used. The measurement uncertainty caused by detection of thermal radiation is reduced from 0.8% to below 0.1% (absorber surface temperature 1200 °C, emissivity 0.9, 500 suns, camera AVT Pike F100B with approximate sensitivity wavelength 0.3–1.0 μm). For lower temperatures or higher solar concentrations, no filter is necessary.

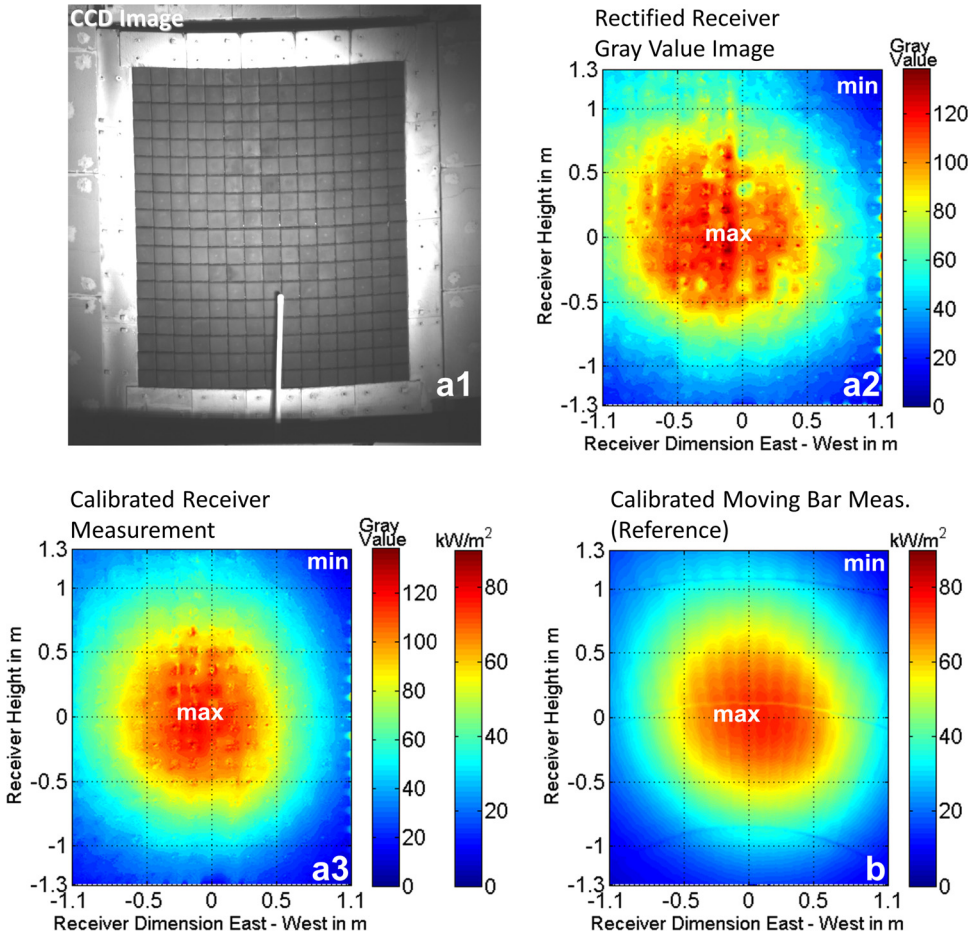

Fig. 2 Grabbed CCD image (*a1*), deskewed and unwinded gray value image in false colors (*a2*), and image after application of brightness correction matrix and calibration (*a3*). Image (*b*) shows the moving bar measurement as reference (open volumetric receiver PSA, ~225 kW, 13.12.07, 13:20 h).

Figure 2(*a1*) shows a CCD image of an open volumetric receiver tested at the PSA. The gray value image shown in Fig. 2(*a2*) was deskewed, unwinded, and the gaps in between the receiver cups are cut out and interpolated from adjacent pixels. As reflectivity of receiver surfaces is usually not homogeneous, significant differences of the light reflected off different receiver cups are observed. A correction matrix to correct spatial variations in hemispherical reflectance must be applied. To derive this matrix, the receiver surface has to be illuminated homogeneously or with a known flux distribution. In this work, ambient light at different meteorological conditions (clouds) is used. Artificial illumination with a known luminosity profile of a stage projector or beamer would be another option. After this correction, the scattering due to inhomogeneous cup reflectivity has been reduced significantly; see Fig. 2(*a3*). Some minor artifacts are still visible caused by varying receiver cup reflectivity over time and nonideal cut out of the gaps between the receiver cups.

Assuming a constant bidirectional reflectance distribution function (BRDF), i.e., a perfect diffusely reflecting material, the corrected gray value distribution can be calibrated to kW/m^2 using a water-cooled Gardon flux gauge. In the tests, it is demonstrated that using more than one flux gauge enhances measurement accuracy, because the nonideally, nonhomogeneously reflecting receiver surface increases calibration uncertainty. Comparing Fig. 2(*a3*) with the reference moving bar measurement Fig. 2(*b*) shows an acceptable agreement, having in mind that the moving bar measures in front of the receiver plane (hence, flux distribution changes) and foci constantly vary due to effects of heliostat tracking and wind.

The assumption of a constant BRDF is only correct for specific angles between receiver, camera, and heliostat and hence is only an approximation. The reflectivity of real receiver surfaces often depends on the ray incidence angle and camera observation angle. For this reason, the receiver material is characterized in a goniореflectometer with a light source at a zenith angle of 14 deg. Figure 3 shows the variation of the normalized BRDF depending on sensor zenith angle and azimuth angle. The sketch inside Fig. 3 illustrates the measurement configuration. Unfortunately, the region of zenith angles between approximately 0 deg to 20 deg cannot be measured, because the light source partly or totally blocks the sensor. However, an increase in the BRDF values around this region can be observed. This indicates a partly retroreflective behavior.

A solar goniореflectometer experiment series has been performed at the CESA-1 tower at the PSA. Assuming Helmholtz reciprocity, the sensor can be exchanged by the camera. For a solar field, this means that the light source position (different heliostat) varies, while the sensor position (camera) is fixed. The camera is positioned at the end of the heliostat field to have free sight to the receiver and not too many nearby heliostats. Groups of heliostats having different angles to the receiver surface are focused subsequently, while during each configuration, CCD images of the receiver surface and moving bar measurements are performed. The ratio of receiver surface brightness (after application of the brightness correction matrix) and brightness of moving bar measurement can be regarded as a normalized BRDF value for the specific configuration. The measurements are also plotted with full markers in Fig. 3. Good agreement with the laboratory goniореflectometer measurements is found.

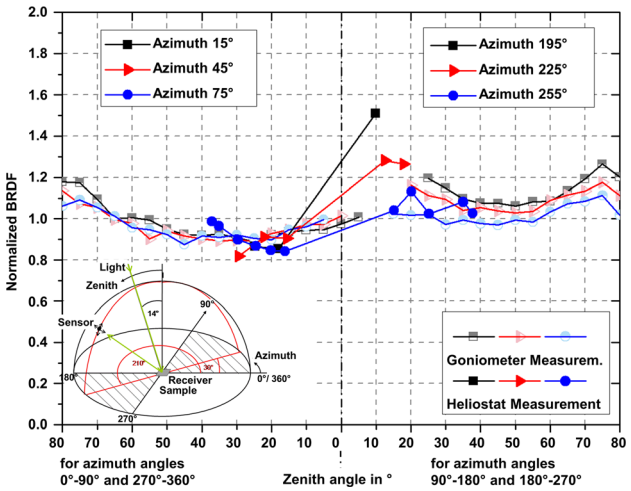

Fig. 3 Normalized BRDF values of a volumetric ceramic receiver as a function of zenith and azimuth angle. Comparison of laboratory gonioreflectometer measurements (sketch left and half markers) and measurements with heliostat groups of solar field (full markers, also see Fig. 4).

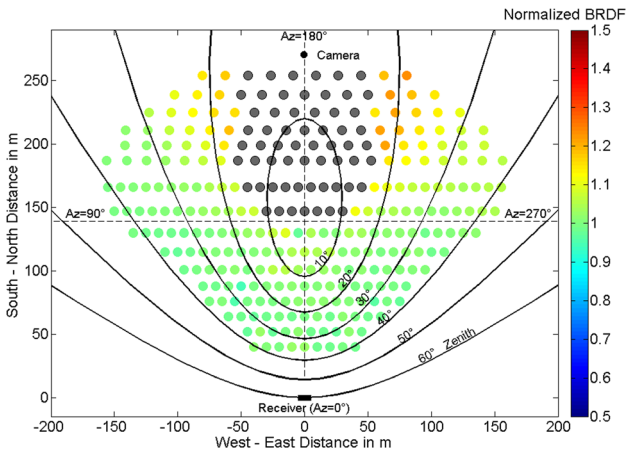

Fig. 4 Normalized BRDF value for each heliostat of the CESA-1 heliostat field at PSA, assuming a plane volumetric air receiver at 84 m height, 30 deg inclined, and camera position at the rear of the field

Indeed, heliostats near the camera position (zenith angle around 10 deg and azimuth angle around 180 deg) have a high BRDF value that exceeds the mean almost by 50%. This means that measuring the light reflected off the receiver coming from these heliostats is overestimated compared to heliostats that are located at zones with lower BRDF values.

Figure 4 shows a map of the CESA-1 heliostat field with isolines of azimuth and zenith angles projected in the heliostat plane. The map is valid for a plane receiver, inclined 30 deg to the vertical at 84 m height above ground, and the camera placed at the rear of the field. The heliostats are colored by their individual normalized BRDF. The values are taken from the laboratory gonioreflectometer measurements of Fig. 3. Heliostats directly nearby the camera are not colored because of lack of measurement data, but one can observe that light from heliostats in the region close to the camera is overestimated, while light from heliostats near the tower is underestimated. The other heliostats represent a mean value and are measured correctly. Consequently, a fixed calibration constant as used in the procedure of Fig. 2 leads only to an approximation of the real flux density distribution. Accuracy can be increased by placing the camera close to the tower and looking upwards as done in the later tests at the Solar Tower Jülich [24].

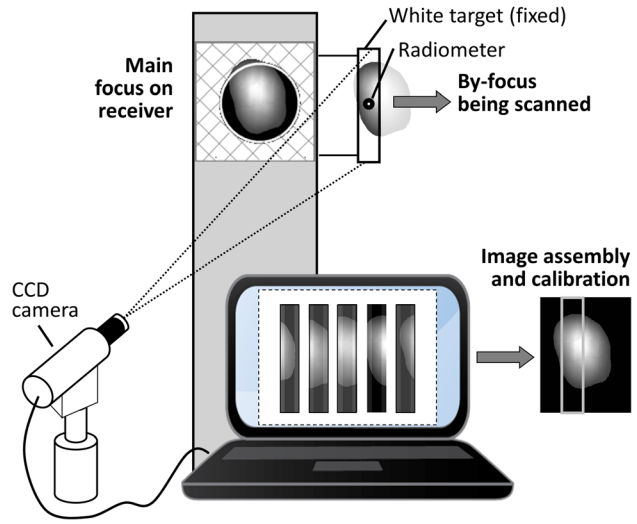

Fig. 5 Procedure of scanning part of the focus over a stripe-shaped, fixed target

This placement avoids the camera to be located directly in the region that is affected by the retroreflective peak.

The authors recommend considering the effect of a nonconstant BRDF. Different calibration constants could be applied, depending on which group of heliostats reflects how much radiation. Applied to practice, this is a challenging task, because external receivers usually are cylindrical and not plane, so one heliostat may have different angles of incidence on the receiver. Additionally, the observation angle of the camera varies over the cylindrical receiver surface. It is planned to use advanced ray tracing software [25] to tackle this challenge in the future. BRDF correction matrices for the actual operating conditions (used heliostats, aimpoint strategies, point of time) will be calculated online during the measurements and the quality of calibration will be increased.

3.3 Flux Density Measurement by Using a Stationary Stripe-Shaped Target and Moving Focus. The concept communicated in Ref. [16] of moving a focus over a stripe-shaped target is further developed. The effect of focus variation due to spatial shift and time past during the measurement is examined in simulations studies, and first tests with single heliostats were performed. Unlike the setup of Ref. [16], a stripe target mounted on the west side of the receiver should be preferred, and instead of moving the whole focus over a water-cooled target at one instance, the authors suggest splitting up the focus in various heliostat groups. For example, 80% still tracks on the receiver, and 20% is swept over the target in various steps. This avoids stopping the receiver operation and the use of an actively cooled target.

The target is stripe-shaped and not squared to reduce wind forces and material costs. It is preferably mounted on the west side of the receiver because of two reasons: Heliostats and the sun move from east to west over the day. Hence, the effect of focus variation due to spatial shift of aimpoint and due to time passed during measurement compensate partly for a target on the west side. A second reason is that if there is any backlash in the gearbox, it has no influence while the heliostat maintains the tracking direction. The bar has to be mounted in a distance to the aperture so that there is no illumination of the target in normal receiver operation to avoid measuring radiation several times.

A CCD image is taken, when the slowest (i.e., usually the nearest) heliostat has reached its new aimpoint. Then, the aimpoint is moved further to take the next image. After the scan of these heliostat groups, the images are assembled together. Before assembling, slight solar irradiation variations during the scan are compensated by weighting each stripe with a DNI value normalized with the DNI during the first image. A flux sensor reading

calibrates the resulting gray value distribution. After evaluating all the heliostat groups, the flux images are added up to get the final result. Figure 5 visualizes the procedure.

The effects of focus variation due to spatial shift of aimpoint and due to time passed during measurement are evaluated by ray tracing simulations. The focus variation due to spatial shift of the aimpoint is mainly caused by changes in cosine losses and optical aberration. The focus variation, caused by the approximately 6 min needed to perform five scans, is due to the varying sun angles and heliostat orientations, leading also to varying cosine losses, optical aberrations, and changing atmospheric attenuation. Both spatial and temporal variations are minimum at solar noon and maximum in the evening and the morning. For a bar target mounted at the west of the tower, these effects compensate to some extent. During morning, due to the spatial focus shift to the west, optical losses increase slightly, while during the 6 min measurement time, the optical losses decrease. At noon, these effects are minimal, and at afternoon, they are vice-versa. At the CESA-1 plant in Almería at 8:00 in the morning, simulations show an uncertainty in the solar flux distribution due to focus variation by spatial shift of aimpoint and the time passed of 1.2%. The uncertainty in integrated power due to focus variation is estimated to 0.5%.

The measurement uncertainties of CCD camera and target are the same as for the ProHERMES system (see Sec. 2). A further, important issue is the accuracy of heliostat tracking and the number of heliostats involved. If tracking errors were too high, the step size in aimpoint shift would not be equal, and the individual images could not be assembled correctly. However, if there are a lot of heliostats involved, then this error compensates to a great extent. In a simulation study, it is shown that with 120 heliostats having a normally distributed tracking error of 0.65 mrad for each axis, a total measurement uncertainty of flux density distribution in the range from −6.0% to +5.5% can be reached. If the tracking error was 1.6 mrad for each axis, measurement uncertainty would increase up to −9.1% to +8.8%. The uncertainty in integrated power is estimated to −4.3% to +3.6%. Individual heliostats have been characterized with this method and a stripe assembling algorithm based on cross correlations to link image stripes using overlap has been developed so far.

3.4 Flux Density Measurement by Using a Moving Bar With Mounted Sensors. Moving bar systems [17,18] equipped with sensors have been presented in Sec. 2. No additional research is performed in this paper for these systems. Issues regarding upscaling of the moving bar for large-scale receivers have already been discussed in Sec. 3.1. Technical solutions for routing of sensor cables from the moving bar to a data acquisition system exist.

3.5 Flux Density Measurement by Using Stationary Sensors. Moving parts are avoided, if several water-cooled flux gauges are distributed in the aperture plane or on the receiver surface and the point measurements are interpolated to flux maps. It is investigated how the number of sensors affects the measurement accuracy. For this, a flux distribution of 46 heliostats focused on one aimpoint around solar noon is used (measured by the ProHERMES system). The location of sensors is defined and the flux values are extracted from the given map. Based on the extracted values, the flux maps are reconstructed by a spline interpolation method. It is shown that the flux distribution and integrated power can be reproduced well using around 25 sensors (grid 5×5) over the flux map. The deviation between reproduced and original integral power is below 0.6%, the rms deviation of the flux distribution relative to the mean flux density on the flux map is 8%. It is shown that using a grid of 16 sensors (grid 4×4), the characteristics of the flux distribution cannot be reproduced totally. In this case, the deviation in integrated power is −3.5%, the rms deviation between reproduced and original flux distribution relative to the mean flux density is 16.8%.

These results cannot be generalized because more complex flux patterns, e.g., with multi-aimpoint strategies, may need more sensors in order to be reproduced correctly. The issues of reliability and lifetime of sensors in high-flux high-temperature regions of receivers have been discussed in Sec. 2.

3.6 Flux Density Distribution by Measurement-Supported Simulation. State-of-the-art ray tracing codes allow a very accurate prediction of the solar flux on any surface. Accuracy of results depend mainly on the quality of input parameters, such as correct representation of concentrator contour errors (slope errors), heliostat tracking errors, heliostat positions and geometry (blocking and shading, cosine effects, optical aberration), mirror reflectivity, atmospheric conditions (DNI, sunshape, atmospheric attenuation), tower geometry (shading), and receiver position. However, the validity of simulation results should be confirmed by measurements, either by an indirect or direct method. These measurements may be reduced significantly in effort compared to the determination of solar flux by measurement only.

During the tests of a solar-hybrid gas turbine system at the PSA [26], results of the ray tracing code STRAL [25] are compared to flux maps produced with the ProHERMES system (moving bar and camera, Sec. 2). The heliostat contour errors taken for the simulations are derived by deflectometry [27]. The exact receiver position relative to the known heliostat field is determined by tachymeter measurements. The measured DNI and an assumed circumsolar ratio of 5%, which is recommended as a single representative value [28], are taken as inputs. The final heliostat reflectivity is chosen in a way that the simulated and the measured solar flux on a radiometer mounted in the receiver area is the same. It is cross-checked with measured values and the deviations are below 2.8%, which is low compared to the uncertainties of DNI and reflectivity measurement, atmospheric extinction, and sunshape. This optional adaption of the heliostat reflectivity might not be feasible in cases where only few heliostats were used or if the radiometer was mounted in a region with high gradients. In our case, the radiometer is mounted on a cooled finger ("coldfinger") in the central plateau region of the focus so that the reading is not influenced significantly by tracking errors.

A major issue is to know the real heliostat aimpoints because the used version of the heliostat control software has not always been working without errors. A random tracking error of $\sigma = 0.9$ mrad for each axis is applied. Figure 6(*a1*) shows the simulated flux distribution on the radiation shield plane. The black circle indicates the receiver aperture that intercepted 266 kW (simulation).

In order to determine whether the simulation result reflects reality, it is compared with the result of an indirect flux measurement method, using a digital camera and the white radiation shield mounted around the aperture surface as target, see Fig. 6(*a2*). Usually, the radiation shield is not perfectly white and not perfectly Lambertian, and in our case, in some parts, there are several round cover panels protruding from the surface that disturb the measurement. To correct spatial variations in local hemispherical reflectance on the radiation shield, a correction matrix is applied to the gray value images of the digital camera, similar to the procedure described in Sec. 3.2. The resulting image is calibrated by radiometers mounted in the measurement surface. The resulting flux distribution is shown in Fig. 6(*a2*). The result is quite promising, although some artifacts of the round cover panels are still observed.

The standard deviation between the simulated (Fig. 6(*a1*)) and measured flux distribution (Fig. 6(*a2*)) on the radiation shield is a measure for the quality of the simulation, more specifically for the congruence of simulated and measured flux distribution. The mean deviation gives information about the goodness of calibration of the measurement and the ray tracing input parameters influencing power like heliostat reflectivity, DNI, or atmospheric attenuation. Mean and standard deviation between simulated and measured flux distribution are calculated for the hatched region. Optimizing the simulations by correcting the global tracking

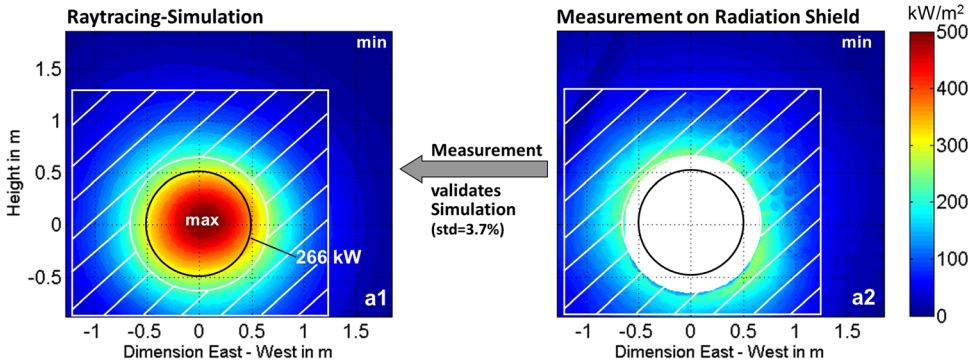

Fig. 6 Flux density distributions on radiation shield plane in kW/m² during test 1 (PSA, 19.05.10, 12:50 h, 46 heliostats). Ray tracing simulation (*a1*). Measurement directly on radiation shield after application of correction matrix and calibration (*a2*).

Table 1 Deviation of flux distribution between simulation (Fig. 6(*a1*)) and measurement on radiation shield (Fig. 6(*a2*)) and resulting simulated receiver input power

Test no.	Mean deviation[a] (%)	Standard deviation[a] (%)	Power[b] (simulated) (kW)
(1): 19.05.2010, 12:50 h	−5.1	3.7	266
(2): 23.06.2010, 12:48 h	2.1	4.5	270

[a]Deviation of simulated and on radiation shield measured flux distribution relative to the mean flux density inside hatched area of Figs. 6(*a1*) and 6(*a2*).
[b]Simulated power incident on receiver aperture area (diameter 0.9 m).

Table 2 Comparison of simulated receiver input power between simulation (Fig. 6(*a1*)) and reference (measurement on moving bar, Fig. 7). Power incident on receiver aperture area (diameter 0.9 m).

Test no.	Power (simulated) (kW)	Power (reference) (kW)	Power deviation (%)
(1): 19.05.2010, 12:50 h	266	265	0.5
(2): 23.06.2010, 12:48 h	270	274	−1.4

offset, for example, reduces the standard deviation. Table 1 reports the values of optimized simulations with minimal standard deviations for two test days. A standard deviation of 3.7% and 4.5% based on the mean flux in the hatched region is reached for the aimpoint-optimized simulation of test no. 1 and no. 2, respectively.

Using the validated simulation, the flux can be evaluated on the aperture surface. The receiver input power determined by integration of the simulated flux distribution is compared to the reference receiver input power in Table 2. The reference input power is taken from the (generally not available) moving bar measurement, Fig. 7. Although the quality of the flux distribution strongly depends on the uncertainty of aimpoints, i.e., the heliostat control system and heliostat tracking accuracy, it can be shown that the solar input power into the aperture can be simulated with a low deviation in the range of about ±2% compared to a moving bar measurement.

Another possibility to validate the simulations is using distributed flux gauges in the receiver aperture, i.e., a direct method. Depending on the number of gauges and the uncertainty of aimpoints, this validation procedure is especially valuable for large-area receivers with a multi-aimpoint strategy and relative small reflection shield surface around the receiver.

The moving bar reference measurement (Fig. 7) is not available normally. In our case, it can serve as an independent confirmation

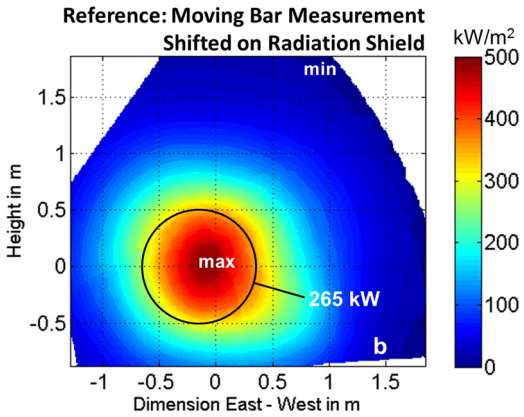

Fig. 7 Moving bar reference measurement shifted to radiation shield plane for test 1, PSA, 19.05.10, 12:50 h

of the measurement-supported simulation result. Because the planes of the moving bar and radiation shield are separated by a distance of about 30 cm, the two results are not directly comparable. To account for this, the reference moving bar measurement result is shifted to the radiation shield plane by using a correction matrix that is generated by dividing the simulated flux distributions of the two planes of interest using the ray tracing results. Comparing the flux distribution of the simulation result (Fig. 6(*a1*)) with the shifted moving bar reference measurement (Fig. 7), a satisfying agreement for the flux distribution and a good agreement for the intercepted power (0.5% deviation) on the receiver aperture is found.

The comparison between the measurement on the radiation shield (Fig. 6(*a2*)) and the moving bar reference (Fig. 7) also shows a satisfying agreement. This indicates that, despite the nonperfect measurement surface of the radiation shield, a measurement on the radiation shield is suitable to check the quality of the simulation.

4 Assessment of Concepts for Large-Scale Receivers

Measurement objectives and design specifications have a major influence on the selection of the preferred concept. Several requirements must be satisfied, which are classified in the categories "necessary" and "desired." The different concepts are compared based on these requirements.

4.1 Catalog of Requirements. Figure 8 shows a visualization of the catalog of requirements. Necessary requirements must be fulfilled in order to be considered in the evaluation: Concepts must measure the desired quantity, must be scalable to large receivers, and must reach a high operational safety for the workers

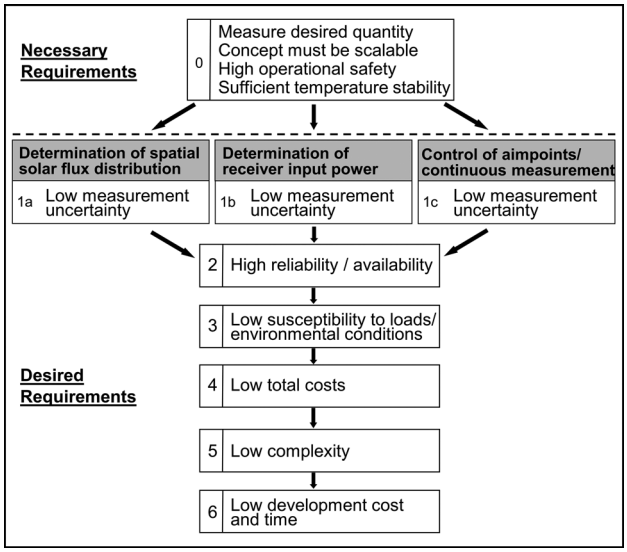

Fig. 8 Requirements to reach the design specifications. The fields marked in gray show the different measurement objectives.

and sufficient temperature stability. The desired requirements should be fulfilled to a maximum, i.e., concepts should have a low measurement uncertainty and a high reliability and availability. Low measurement uncertainty is desired for the determination of (a) spatial solar flux distribution on the receiver surface, (b) receiver input power, e.g., for acceptance testing, and (c) continuous measurement to deliver input to an aimpoint control system. While the first two measurements may only be needed at some specific points in time, but with high measurement accuracy, input for an aimpoint control system must be available continuously, but with lower accuracy. As a consequence, the concepts should be evaluated regarding their measurement objective individually. Besides low measurement uncertainty, the system should have high system reliability and availability, and low susceptibility to the operational loads and environmental conditions (e.g., wind, humidity, rain, dust). The investment, maintenance, and operating costs should be low. This can be reached, e.g., by maximizing the use of standard parts that comply with the other mentioned requirements. The technical complexity of the system should be low, and it should be easy to operate. The development cost and time also should be modest.

4.2 Comparison of Concepts. The different concepts are evaluated regarding the catalog of requirements taking into account the three measurement objectives (1a) to (1c) of Fig. 8. Table 3 shows the scores of the individual requirements and the weighted sums calculated as

$$\text{Weighted sum} = \Sigma(\text{Score of requirement } i \times \text{weighting factor } i)$$

Necessary requirements are fulfilled completely by all systems, so they do not appear in the table. In the lower part of Table 3, the weighted sum is listed individually for each measurement objective (1a)–(1c) and one value for all measurement objectives. The latter is calculated by the same weighting procedure only that in a first step, the scores of the individual measurement objectives of the requirement "low measurement uncertainty" are averaged without weighting.

For the column "direct measurement with distributed stationary sensors (Sec. 3.5)," two scores are given, depending on the numbers of sensors used. A higher number of sensors increases measurement accuracy but also increases the costs and complexity. Also two scores are listed in each of the two columns of measurement-supported simulations (Sec. 3.6). The first score assumes that the heliostat aimpoints are known with sufficient accuracy, i.e., a state-of-the-art aimpoint control with good heliostats is installed. Then, the size of the radiation shield measurement area compared to the receiver area may be small or the number of flux sensors may be low while still a low measurement uncertainty is guaranteed. The second score is given, if the heliostat aimpoint system does not work properly. In this case, the best simulation run out of multiple runs with different statistical aimpoint distributions would be chosen. More flux sensors or a larger irradiated radiation shield surface would be needed to do this.

The following paragraphs explains the scoring of each requirement. The measurement uncertainty of the solar flux distribution (requirement 1a) is lowest for the moving bar with camera (Sec. 3.1), followed by the moving bar with sensors (Sec. 3.4). The measurement-supported techniques (Sec. 3.6) can also provide good-quality solar flux distributions in case of a good knowledge of real heliostat aimpoints. A little higher uncertainty has the measurement on the external receiver surface (Sec. 3.2) due to the non-Lambertian properties and inhomogeneities in reflectivity of the receiver, the moving focus over a fixed bar (Sec. 3.3), and distributed stationary sensors (Sec. 3.5). More details can be found in Secs. 2 and 3.

The receiver input power is determined by integration of a flux map so that uncertainties in the flux distribution have a lower influence on the integrated power and can be accepted, as long as the calibration of the flux map is valid. For this, regarding low measurement uncertainty (requirement 1b), all scores for the receiver input power are better or equal than for the flux distribution. The measurement-supported simulations (Sec. 3.6) may have some issues with the correct calibration of the simulated map (e.g., uncertainties in field reflectivity set as boundary condition in the simulation).

The measurement uncertainty regarding aimpoint control (requirement 1c) is good for the moving bar technologies (Secs. 3.1 and 3.4) but not excellent because they measure in a plane in front of the receiver aperture and they cannot measure continuously. The measurement on the external receiver surface (Sec. 3.2) is excellent in this point. The moving focus over a stationary bar (Sec. 3.3) takes heliostats out of the focus and moves the aimpoints, so it is not recommended for their control. Distributed stationary sensors (Sec. 3.5) provide a continuous flux density signal, and, if their number is high enough, a good input for aimpoint control. Also the measurement-supported simulations (Sec. 3.6) realized in real-time can provide good input for an aimpoint control especially if connected with some distributed sensors.

Regarding the reliability and, hence, the availability of the measurement system (requirement 2), the mechanical moving bar techniques are good (Secs. 3.1 and 3.4), if they are designed and maintained well, but a few outages may occur. Many distributed sensors in the high-flux high-temperature zone (Sec. 3.5) of a receiver may be critical and their reliability is poor as stated in Sec. 2. The measurement-supported simulations (Sec. 3.6) usually do not have issues regarding system outages (except for the sensors if used. Regarding requirement 3, mechanical moving bars (Secs. 3.1 and 3.4) are more susceptible to ambient conditions as wind, rain, humidity, and thermal loads as the sensors used in the other techniques. Regarding costs (requirement 4), installation and maintenance of moving bars (Secs. 3.1 and 3.4) or many water-cooled sensors in the receiver (Secs. 3.5 and 3.6) are more expansive than measurement techniques without extra installations. Regarding complexity (requirement 5), moving bar systems (Secs. 3.1 and 3.4) are more complex than other systems, but the complexity can be handled by a good design. The distributed sensor system (Sec. 3.5), which requires the installation, wiring, and water-cooling of many water distributed sensors inside a radiated high-temperature receiver, is considered as complex. The measurement-supported simulation with sensors (Sec. 3.6) should need much less sensors. The development status of the

Table 3 Evaluation of different solar flux measurement techniques. ++ excellent (+2), + good (+1), o fair (0), − poor (−1), and −−very poor (−2).

	Moving bar technology		Technologies without moving bar				
Method Short description	Indirect Moving bar target, camera	Direct Moving bar with sensors	Indirect External receiver surface, camera	Indirect Stationary bar target, moving focus, camera	Direct Distributed stationary sensors	Simulation—indirect Supported by radiation shield meas., camera	Simulation—direct Supported by measurement with sensors
Section	(3.1)	(3.4)	(3.2)	(3.3)	(3.5)	(3.6)	(3.6)
Applicable to[a]	A, B, C	A, B, C	B, C	A, B	A, B, C	A, B	A, B, C
1 Low measurement uncertainty (weight: 50)							
1a: Solar flux distribution	++	+	o	o	o/−[b]	+/o[c]	+/o[c]
1b: Receiver input power	++	++	+	+	+/o[b]	+/o[c]	+/+[c]
1c: Aimpoint control	+	+	++	−	+/o[b]	+/o[c]	++/+[c]
2 High availability/reliability (weight: 20)	+	+	++	+	o	++	+
3 Low susceptibility to loads/environment (weight: 10)	o	o	+	+	+	+	+
4 Low total costs (weight: 10)	o	o	++	+	o/+[b]	+	+/o[d]
5 Low complexity (weight: 5)	+	+	++	++	o/+[b]	++	++
6 Low development cost and time (weight: 5)	+	+	+	o	+	+	+
→ Weighted sum: excellent (>150); good [100;150]; fair [50;100]; poor [0;50]; very poor (<0)							
1a: Solar flux distribution	130	80	90	50	20/−20	130/80	110/50
1b: Receiver input power	130	130	140	100	70/30	130/80	110/100
1c: Aimpoint control	80	80	190	0	70/30	130/80	160/100
All: 1a–1c	110	100	140	50	50/10	130/80	120/80

[a]Measurement technique applicable to receiver types: A, cavity; B, external north facing; and C, external surround.
[b]Using many/only few measurement sensors.
[c]With good/poor knowledge of heliostat aimpoints.
[d]Using few/many measurement sensors.

technologies is not so different except for the moving focus over a stationary bar where still some software and tracking issues must be solved to get a proper composite image (requirement 6).

Evaluating the scores, we get the following results. One good option to measure the spatial solar flux distribution (measurement objective 1a in Fig. 8) is the moving bar technique with digital camera (Sec. 3.1). A linearly moving bar is evaluated as more feasible than a rotating bar for large-area receivers. Currently, a linear moving bar is designed. A further suitable technique for flux distributions is the measurement-supported simulation preferably using a flux camera for the radiation shield or, if not possible, some distributed stationary flux sensors (Sec. 3.6), assuming a state-of-the-art heliostat aimpoint system. Not recommended for measuring flux distributions on large-scale receivers is the technique to use distributed stationary sensors only (Sec. 3.5), because of lifetime and reliability reasons and the large numbers required (costs and complexity) to reach reasonable accuracy in interpolating between them. The other techniques are in the middle of the rankings.

The receiver input power (measurement objective 1b in Fig. 8) is determined by integrating the solar flux distribution. Additionally to the moving bar technique with digital camera (Sec. 3.1) and the measurement-supported simulation using either the camera based radiation shield measurement or distributed stationary flux sensors (Sec. 3.6), the moving bar with sensors (Sec. 3.4) and the measurement on external receiver surface (Sec. 3.2), if applicable, are suitable for this task. The other techniques are in the middle of the rankings, depending on the particular conditions.

A very good technique for aimpoint control and continuous measurements (objective 1c in Fig. 8) is the measurement on the external receiver surface (Sec. 3.2), if applicable. Not recommended for aimpoint control is the technique using a stationary bar target and a moving focus (Sec. 3.3), because aimpoints are moved, measurement takes some minutes, and receiver power is reduced. The other systems can all be used for aimpoint control, depending on the particular conditions. Especially the measurement-supported simulations (Sec. 3.6) assuming a state-of-the-art heliostat aimpoint system have potential here.

5 Conclusion

In general, the direct and indirect moving bar techniques (Secs. 3.1 and 3.4) are attractive due to their low measurement uncertainty in all measurement tasks. However, the mechanical moving bar causes more costs and may have a higher susceptibility to loads and environment. The opposite occurs with the measurement on the external receiver surface (Sec. 3.2). It has a higher uncertainty for the flux distribution and good accuracies in the other two tasks, but it is technologically simple. The technique using a stationary bar target and a moving focus (Sec. 3.3) may deliver reasonable receiver input power but is not recommended for aimpoint control or to measure the flux distribution. The distributed stationary sensors technique (Sec. 3.5) is good for measuring receiver input power and for aimpoint control, if a sufficient number of sensors is used, but has reliability and cost issues. The measurement-supported simulation techniques (Sec. 3.6) score with high reliability, low susceptibility to loads and environment, low costs, and low complexity but need close to ideal conditions to achieve low uncertainties.

Acknowledgment

Financial support from the German Federal Ministry for the Environment, Nature Conservation and Nuclear Safety (Contract

No. ZIII5-16UM0068) and the European Union (Contract Nos. 019830 and 219110) is gratefully acknowledged. The authors also thank Olaf Bender, Janina Nettlau, Markus Pfänder, Jan-Peter Säck, Tamara Schapitz, Björn Schiricke, Reiner Schlee, and Ralf Uhlig for their valuable contributions.

References

[1] Thalhammer, E., 1979, "Heliostat Beam Characterization System—Update," I.S.A. Reprint 79-692, ISA-79 National Conference and Exhibit, Chicago, Illinois.
[2] von Tobel, G., Schelders, Ch., and Real, M., 1982, "Concentrated Solar Flux Measurements at the IEA-SSPS Solar Central Receiver Power Plant," Tabernas—Almería, Spain, Final Report, Swiss.
[3] Schiel, W., 1985, "500 kW-Solarturmkraftwerk—Teil I: Mess-Grössen und Messsystem," Brennstoff-Wärme-Kraft (BWK) 6/85, S. 266–268.
[4] Neumann, A., and Monterreal, R., 1992, "Measurement of Concentrated Solar Radiation With the HERMES II System at the PSA," 6th International Symposium on Solar Thermal Concentrating Technologies, Mojacar, Spain, Sept. 28–Oct. 2.
[5] Lüpfert, E., Heller, P., Ulmer, S., Monterreal, R., and Fernández, J., 2000, "Concentrated Solar Radiation Measurement With Video Image Processing and Online Fluxgage Calibration," Solar Thermal 2000 International Conference, Sydney, Australia, Mar. 8–10.
[6] Imenes, A., Stein, W., Hinkley, J., Benito, R., Bolling, R., Schramek, P., and Ulmer, S., 2006, "Ray Tracing and Flux Mapping as a Design and Research Tool at the National Solar Energy Centre," ANZSES 2006 Conference (Australia and New Zealand Solar Energy Society), Canberra, Australia, Sept. 13–15, Paper No. S06-81.
[7] Neumann, A., and Groer, U., 1996, "Experimenting With Concentrated Sunlight Using the DLR Solar Furnace," Solar Energy, **58**, pp. 181–190.
[8] Kröger, K., Kaluza, J., and Neumann, A., 2000, "First Application of the Flux Mapping System SCATMES for Secondary Concentrator Performance Analysis," Solar Thermal 2000 International Conference, Sydney, Australia.
[9] Giral, J., Boulet, N., and Hernandez, G., 2000, "OBELIX: Flux Mapping System Using a Video Camera," Proceedings of the 14th Task III Meeting Within IEA SolarPACES on Solar Technology and Applications, Sydney, Australia SolarPACES Technical Report No. III-2/00.
[10] Johnston, G., 1994, "Focal Region Characterizations of Paraboloidal Dishes at the Australian National University," Proceedings of Seventh International Symposium on Solar Thermal Concentrating Technologies, Moscow, Sept. 26–30.
[11] Ulmer, S., Reinalter, W., Heller, P., Lüpfert, E., and Martinez, D., 2002, "Beam Characterization and Improvement With a Flux Mapping System for Dish Concentrators," ASME J. Sol. Energy Eng., **124**(2), pp. 182–188.
[12] Ulmer, S., 2004, "Messung der Strahlungsflussdichte-Verteilung Von Punktkonzentrierenden Solarthermischen Kraftwerken," Ph.D. dissertation, VDI Verlag, Düsseldorf.
[13] Ulmer, S., Lüpfert, E., Pfänder, M., and Buck, R., 2004, "Calibration Corrections of Solar Tower Flux Density Measurements," Energy, **29**(5–6), pp. 925–933.
[14] Strachan, J. W., and Houser, R. M., 1993, "Testing and Evaluation of Large-Area Heliostats for Solar Thermal Applications," Sandia National Laboratories, Albuquerque, NM, SAND92-1381, UC-235.
[15] Ho, C., and Khalsa, S., 2012, "A Photographic Flux Mapping Method for Concentrating Solar Collectors and Receivers," ASME J. Sol. Energy Eng., **134**(4), p. 041004.
[16] Pacheco, J., Houser, R., and Neumann, A., 1994, "Concepts to Measure Flux and Temperature for External Central Receivers," Joint Solar Engineering Conference, ASME, pp. 595–603.
[17] Ballestrín, J., and Monterreal, R., 2004, "Hybrid Heat Flux Measurement System for Solar Central Receiver Evaluation," Energy, **29**(5–6), pp. 915–924.
[18] Yogev, O., Gleckman, P., and Rozler, M., 2009, "High-Heat Solar Flux Scanner," Proceedings of SolarPACES 2009, Berlin, Germany, Sept. 15–18.
[19] Elsayed, M. M., Fathalah, K. A., and Al-Rabghi, O. M., 1995, "Measurements of Solar Flux Density Distribution on a Plane Receiver due to a Flat Heliostat," Sol. Energy, **54**(6), pp. 403–411.
[20] Osuna, R., Morillo, R., Jiménez, J. M., and Fernández-Quero, V., 2006, "Control and Operation Strategies in PS10 Solar Plant," Proceedings 13th Solar PACES, Sevilla, Spain, Jun. 20–23.
[21] Lewandowski, A., Bingham, C., Rouzine, M., and Rouzine, A., 2000, "Testing of a Wire Analyzer for Flux Distribution," Solar Thermal 2000 International Conference, Sydney, Australia, Mar. 8–10.
[22] Kaluza, J., and Neumann, A., 2001, Comparative Measurements of Different Solar Flux Gauge Types," ASME J. Sol. Energy Eng., **123**(3), pp. 251–255.
[23] Ballestrín, J., Estrada, C. A., Rodríguez-Alonso, M., Pérez-Rábago, C., Langley, L. W., and Barnes, A., 2006, "Heat Flux Sensors: Calorimeters or Radiometers?," Sol. Energy, **80**, pp. 1314–1320.
[24] Göhring, F., Bender, O., Röger, M., Nettlau, J., and Schwarzbözl, P., 2011, "Flux Density Measurement on Open Volumetric Receivers," Proceedings of SolarPACES 2011, Granada, Spain, Sept. 20–23.
[25] Belhomme, B., Pitz-Paal, R., Schwarzbözl, P., and Ulmer, S., 2009, "New Fast Ray Tracing Tool for High-Precision Simulation of Heliostat Fields," ASME J. Sol. Energy Eng., **131**(3), p. 031002.
[26] Amsbeck, L., Denk, T., Ebert, M., Gertig, C., Heller, P., Herrmann, P., Jedamski, J., John, J., Pitz-Paal, R., Prosineĉki, T., Rehn, J., Reinalter, W., and Uhlig, R., 2010, "Test of a Solar-Hybrid Microturbine System and Evaluation of Storage Deployment," Proceedings of SolarPACES 2010, Perpignan, France, Sept. 21–24.
[27] Ulmer, S., März, T., Prahl, C., Reinalter, W., and Belhomme, B., 2011, "Automated High Resolution Measurement of Heliostat Slope Errors," Sol. Energy, **85**, pp. 681–687.
[28] Neumann, A., Witzke, A., Jones, S., and Schmitt, G., 2002, "Representative Terrestrial Solar Brightness profiles," ASME J. Sol. Energy Eng., **124**(2), pp. 198–204.